



## Hot deformation behavior of Al–9.0Mg–0.5Mn–0.1Ti alloy based on processing maps

Cai-he FAN<sup>1,2</sup>, Ying-biao PENG<sup>1</sup>, Hai-tang YANG<sup>1</sup>, Wei ZHOU<sup>1</sup>, Hong-ge YAN<sup>2,3</sup>

1. College of Metallurgy and Material Engineering, Hunan University of Technology, Zhuzhou 412007, China;

2. Hunan Provincial Key Laboratory of Spray Deposition Technology and Application,  
Hunan University, Changsha 410082, China;

3. College of Materials Science and Engineering, Hunan University, Changsha 410082, China

Received 18 August 2016; accepted 30 December 2016

**Abstract:** Hot deformation behavior of extrusion preform of the spray-formed Al–9.0Mg–0.5Mn–0.1Ti alloy was studied using hot compression tests over deformation temperature range of 300–450 °C and strain rate range of 0.01–10 s<sup>-1</sup>. On the basis of experiments and dynamic material model, 2D processing maps and 3D power dissipation maps were developed for identification of exact instability regions and optimization of hot processing parameters. The experimental results indicated that the efficiency factor of energy dissipate ( $\eta$ ) lowered to the minimum value when the deformation conditions located at the strain of 0.4, temperature of 300 °C and strain rate of 1 s<sup>-1</sup>. The softening mechanism was dynamic recovery, the grain shape was mainly flat, and the portion of high angle grain boundary (>15°) was 34%. While increasing the deformation temperature to 400 °C and decreasing the strain rate to 0.1 s<sup>-1</sup>, a maximum value of  $\eta$  was obtained. It can be found that the main softening mechanism was dynamic recrystallization, the structures were completely recrystallized, and the portion of high angle grain boundary accounted for 86.5%. According to 2D processing maps and 3D power dissipation maps, the optimum processing conditions for the extrusion preform of the spray-formed Al–9.0Mg–0.5Mn–0.1Ti alloy were in the deformation temperature range of 340–450 °C and the strain rate range of 0.01–0.1 s<sup>-1</sup> with the power dissipation efficiency range of 38%–43%.

**Key words:** spray forming; Al–9.0Mg–0.5Mn–0.1Ti alloy; hot compressing deformation; processing map; dynamic recrystallization

### 1 Introduction

Of excellent properties such as well corrosion resistance, good welding performance and high integrated mechanical properties, Al–Mg alloy has long been considered as an attractive material in automotive, shipping and aerospace industries [1–3]. However, it is difficult to obtain high strength and high toughness properties by using conventional casting method [4] due to the coarse grain and dendrite segregation caused by low cooling rate. Spray forming technology is recognized as an ideal method to prepare high Mg content Al–Mg alloy with high cooling rate, large content of solute Mg, fine grains without macro segregation [5]. Compared with as-cast alloy, the spray-formed Al–Mg alloy is more difficult to hot-compression deform due to the high solute Mg content and some

defects such as porosity in the alloy [6]. It is significant to establish reasonable processing and basic parameters before plastic processing (e.g., the flow stress) [7,8]. In recent years, many researchers [9–12] have investigated the microstructure evolution and flow stress behavior of Al–Mg alloys during the hot compression process. The processing map technique has been widely used to understand the hot deformation behavior of various metals, including Al-alloy [13], Mg-alloy [14] and Ti-alloy [15], and so on. WANG et al [12] studied the flow stress behavior of spray-formed 5A06 aluminum alloy during hot compression process. LIU et al [16] investigated the metal workability of AZ31B magnesium alloy using 3D processing map. SUN et al [17] studied the hot deformation behavior of TiAl-based alloy prepared through powder metallurgy using 3D processing map.

In this study, the isothermal hot compression test in

the Gleeble–3500 machine was used to investigate the flow stress behavior of spray-formed Al–9.0Mg–0.5Mn–0.1Ti alloy in a wide range of deformation temperature, strain and strain rate. The main objectives of the present work are 1) to propose the 2D processing maps and 3D power dissipation maps for the hot deformation of spray-formed Al–9.0Mg–0.5Mn–0.1Ti alloy based on the experimental results of isothermal hot compression tests, and 2) to analyze the instability region and optimize the hot deformation parameters. In the present work, 2D processing maps and 3D power dissipation maps were employed to explore the deformation mechanisms along with the microstructure manifestations during the hot deformation process so as to realize the microstructure control.

## 2 Experimental

The deposit preform of Al–9.0Mg–0.5Mn–0.1Ti alloy was produced by self-developed spray forming machine (SD380). The chemical composition (mass fraction, %) of the deposit preform was as follows: 9.0% Mg, 0.5% Mn, 0.1% Ti and 90.4% Al. The plates with the section size of 12 mm×100 mm were extruded from the deposit preform at the extrusion temperature of 450 °C and extrusion ratio of 15:1. The microstructure of the plate materials is shown in Fig. 1. It can be seen that the microstructure of the alloy after extruding is non-uniform, exhibiting a strip-like structure with coarse grains. The strip-like grains mainly exist in the outer region, which is caused by high extrusion temperature and non-uniform deformation. All the compression-testing specimens of 8 mm in diameter and 12 mm in height were machined with their cylinder axes perpendicular to the surface of the plate materials. The metallographic specimens were corroded by the mixture of 2 mL HF, 3 mL HCl, 5 mL HNO<sub>3</sub> and 250 mL H<sub>2</sub>O after grinding and polishing and then drying. The microstructure of the specimen was characterized by optical microscopy (OM).

In order to study the hot compressive behavior, isothermal and constant-strain rate compression tests were carried out on a Gleeble–3500 testing system at temperatures of 300, 350, 400 and 450 °C and strain rates of 0.01, 0.1, 1, 5 and 10 s<sup>-1</sup>. Before the compression tests, the specimens were heated to the deformation temperature with the heating rate of 5 °C/s and held for 3 min to obtain uniform deformation temperature, and then deformed to a true strain of 0.8. During the testing process, the actual temperature of the specimen was controlled within ±2 °C using thyristor controlled three zone furnace. The true strain rate was controlled by exponential decay of the ram speed with time. Both ends of the cylinder sample were daubed with lubricant with

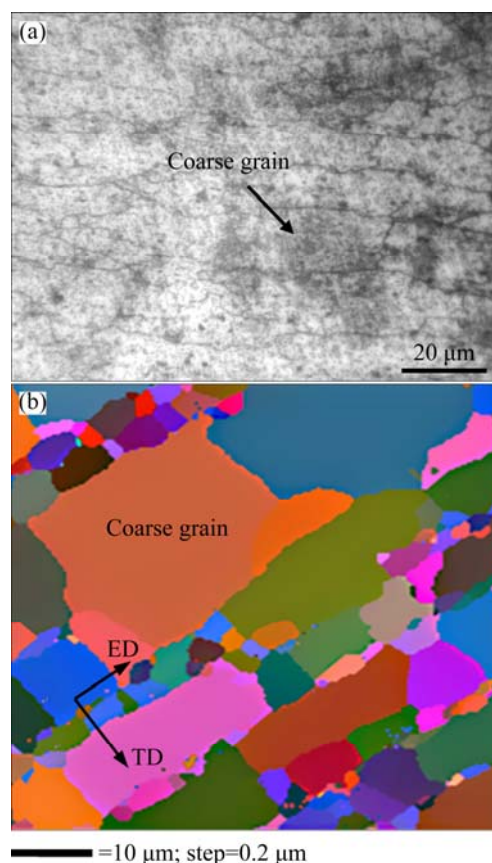


**Fig. 1** Optical image (a) and EBSD map (b) of spray-formed Al–9.0Mg–0.5Mn–0.1Ti alloy extruded at 450 °C (ED—Extrusion direction; TD—Traverse direction)

the chemical component of 75% graphite, 20% engine oil and 5% nitric acid from mesitylene fat. The variations of stress and strain were monitored continuously using a personal computer equipped with an automatic data acquisition system. The true stress and true strain were derived from the measurement of the nominal stress–strain relationship. After the compression test, in order to reserve the hot-deformed microstructure for optical observation, the specimens were water quenched with the delay time less than 5 s. Electron backscattered diffraction (EBSD, Helios Nanolab 600i-SEM) was employed to investigate the microstructure evolution of the deformed specimen. The samples for EBSD observation were prepared on sections parallel to the compression axis. The EBSD samples were prepared by electro polishing method using a solution of 80% C<sub>2</sub>H<sub>5</sub>OH and 20% HClO<sub>4</sub> at 20 V for 30 s. The EBSD samples were analyzed by TSL OIM software, performing at 20 kV and 70° tilt with 0.2 μm scan steps.

## 3 Results and discussion

### 3.1 Flow behavior

The true stress–true strain curves of the extrusion

preform of the spray-formed Al–9.0Mg–0.5Mn–0.1Ti alloy compressed at 300–450 °C and various strain rates are shown in Fig. 2. It can be seen that the flow stress curves exhibit similar characteristics at the early stages of deformation process. The flow stress presents a tendency of a sharp increase up to a peak stress at a quite small strain. When the strain rate is lower than  $1 \text{ s}^{-1}$ , the flow stress firstly reaches a maximum value with the increase of strain, and then gradually decreases to a slightly lower value and maintains at this value no matter how much the strain would be, as can be seen in Figs. 2(a) and (b). When the strain rate is equal to  $1 \text{ s}^{-1}$ ,

different relationships between the flow stress and strain can be observed at various temperatures, as shown in Fig. 2(c). However, the flow stress fluctuates instead of keeping constant when the strain rate is higher than  $1 \text{ s}^{-1}$ , as shown in Figs. 2(d) and (e). This phenomenon is mainly attributed to the rapid increase of the dislocation density during the early stage of deformation process. On the one hand, the flow stress increases sharply with the increase of strain, which leads to the work hardening of the alloy. On the other hand, with the continuous increase of deformation, the dynamic recovery and crystallization take place, which will soften the alloy. As a result, serrate

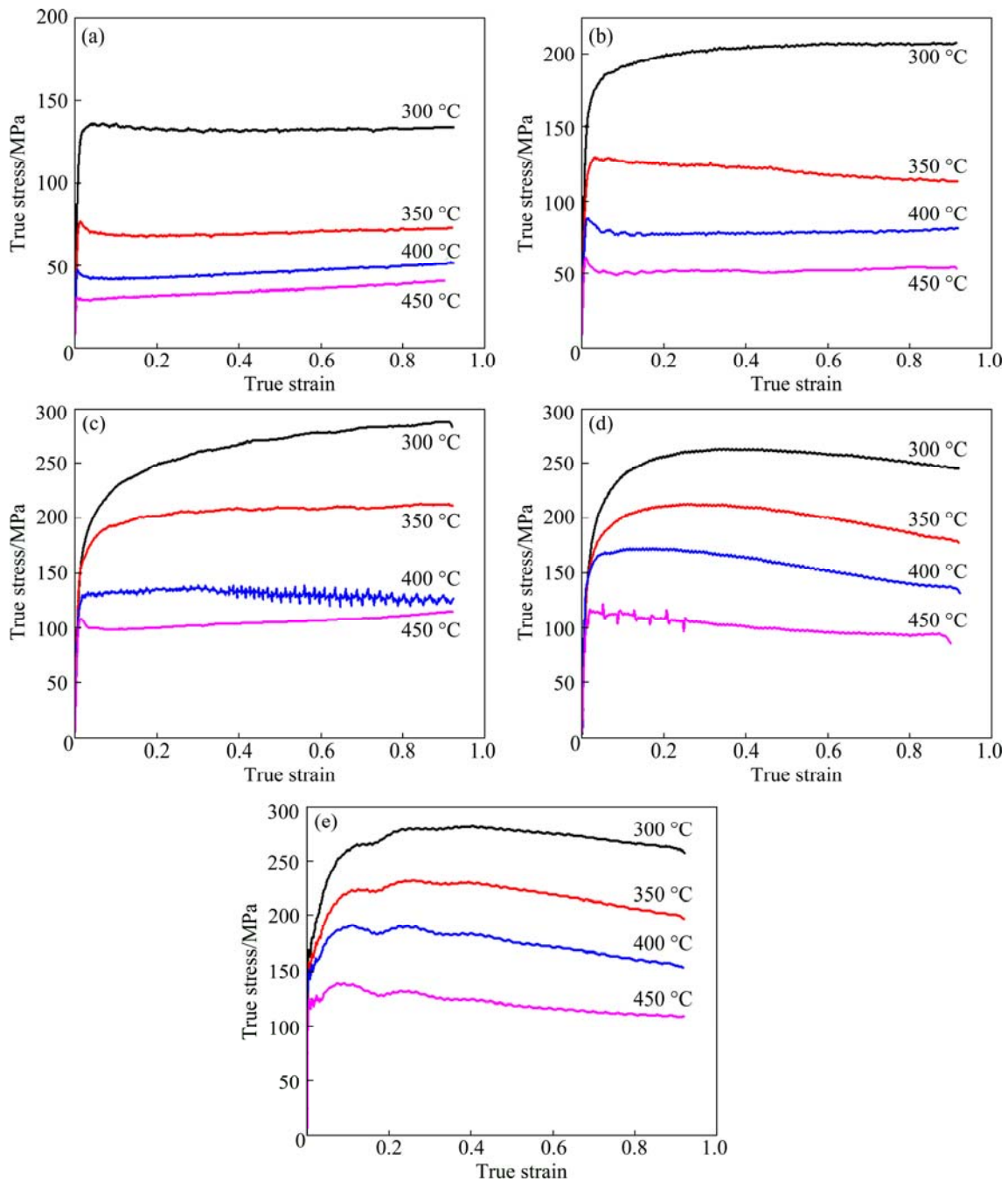


**Fig. 2** True stress–true strain curves of spray-formed Al–9.0Mg–0.5Mn–0.1Ti alloy at different deformation temperatures and strain rates: (a)  $\dot{\epsilon} = 0.01 \text{ s}^{-1}$ ; (b)  $\dot{\epsilon} = 0.1 \text{ s}^{-1}$ ; (c)  $\dot{\epsilon} = 1 \text{ s}^{-1}$ ; (d)  $\dot{\epsilon} = 5 \text{ s}^{-1}$ ; (e)  $\dot{\epsilon} = 10 \text{ s}^{-1}$

fluctuations appear due to the above integrated effects. As the dynamic equilibrium between the softening and hardening mechanism is reached in the process of alloy deformation, the flow stress will maintain to be a stable value. It can be concluded that the flow behaviors of Al–9.0Mg–0.5Mn–0.1Ti alloy are greatly influenced by deformation temperature, strain rate and strain.

### 3.2 Computation of parameters $m$ and $\eta$

The approach of processing map based on the principles of dynamic materials model (DMM), which was proposed by GEGEL et al [18], was employed to study the deformation behavior of the experimental alloys at elevated temperatures. This model can not only associate the microstructure evolution with the deformation mechanisms, but also successfully describe the dynamic recovery area of the materials during the hot compression process. In this model, the materials under hot compression conditions are considered to be a power dissipater ( $P$ ), which can be divided into two parts of  $G$  and  $J$ , as follows:

$$P = \sigma \dot{\epsilon} = G + J = \int_0^{\dot{\epsilon}} \sigma d\dot{\epsilon} + \int_0^{\sigma} \dot{\epsilon} d\sigma \quad (1)$$

where  $G$  is the energy consumed by plastic deformation and  $J$  is the energy consumed by microstructure evolution. The distribution between  $G$  and  $J$  is determined by the strain rate sensitivity exponent  $m$ . It is calculated as a function of strain rate ( $\dot{\epsilon}$ ). The  $\ln \sigma$  versus  $\ln \dot{\epsilon}$  data are fitted by a cubic spline. According to the experimental data, the curves of  $\ln \sigma - \ln \dot{\epsilon}$  can be obtained, as shown in Fig. 3.

$$m = \left[ \frac{\partial J}{\partial G} \right]_{\epsilon, T} = \left[ \frac{\dot{\epsilon} \partial \sigma}{\sigma \partial \dot{\epsilon}} \right]_{\epsilon, T} = \left[ \frac{\partial (\ln \sigma)}{\partial (\ln \dot{\epsilon})} \right]_{\epsilon, T} \quad (2)$$

Generally, the strength of any metallic material increases with the increase of plastic strain rate [18]. The rate sensitive flow behavior is given as follows:

$$\sigma = K \dot{\epsilon}^m \quad (3)$$

where  $\sigma$  is the flow stress and  $\dot{\epsilon}$  is the strain rate.  $K$  is a parameter which depends upon the structure of the material and deformation temperature. At any given deformation temperature,  $J$  can be evaluated by integrating the following equation:

$$J = \int_0^{\sigma} \dot{\epsilon} d\sigma = \frac{m\sigma\dot{\epsilon}}{m+1} \quad (4)$$

where  $m$  is the sensitivity factor of strain rate, the value of  $m$  varies from 0 to 1. When the alloy stays at an ideal dissipation state,  $m$  equals 1 and the value of  $J$  reaches a maximum value ( $J_{\max} = \sigma\dot{\epsilon}/2$ ). As for the nonlinear dissipation, the power dissipation characteristics of the material can be reflected by power dissipation efficiency

$\eta$  [18], which is given by

$$\eta = \frac{J}{J_{\max}} = \frac{2m}{m+1} \quad (5)$$

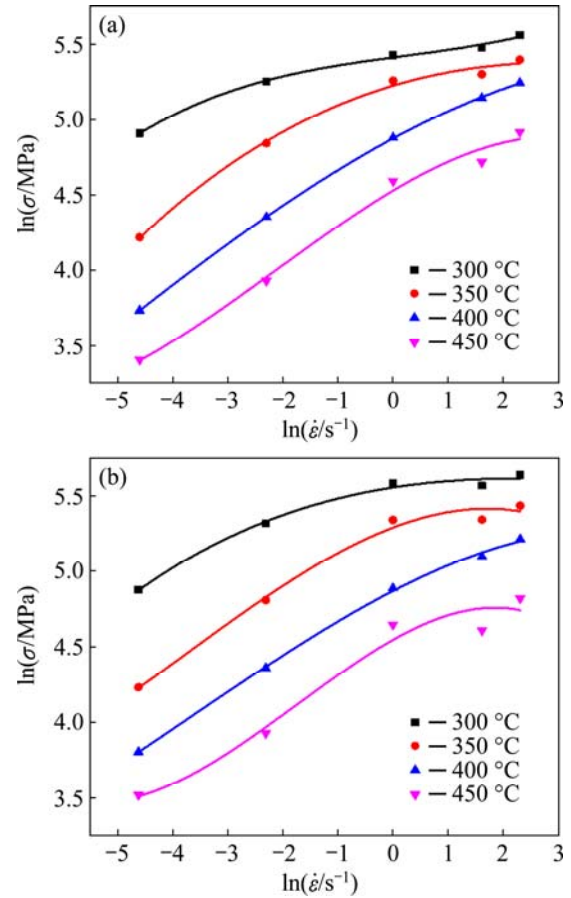


Fig. 3 Relationship between flow stress and strain rate under strains of 0.2 (a) and 0.4 (b)

The variation of  $\eta$  is perhaps correlated with the specific microstructure evolution mechanisms. The parameter  $\eta$  represents the proportion of the power dissipated by microstructure evolution to total power. Generally,  $\eta$  is used to indicate the dissipation of powder induced by the microstructure evolution of the material [16]. However, WANG et al [19] found in Al–Si alloy that the highest  $\eta$  does not necessarily mean better workability. Thus, according to the principle of irreversible thermodynamics, it is necessary to define another dimensionless parameter ( $\xi(\dot{\epsilon})$ ) for the rheological instability criterion in the large deformation process of material [18]:

$$\xi(\dot{\epsilon}) = \frac{\partial \ln \left( \frac{m}{m+1} \right)}{\partial \ln \dot{\epsilon}} + m \leq 0 \quad (6)$$

where  $\xi(\dot{\epsilon})$  is the instability parameter. The relationship curve between  $\ln[m/(m+1)]$  and  $\ln \dot{\epsilon}$  was drawn according to the experimental data, as shown in Fig. 4, which represents the direct relationship between

the value of  $\xi(\dot{\epsilon})$  and the deformation parameters including temperature, strain rate and the strain as the value of  $\xi(\dot{\epsilon})$  is negative. Therefore, a processing map can be built by superimposing the instability map over the power dissipation map.

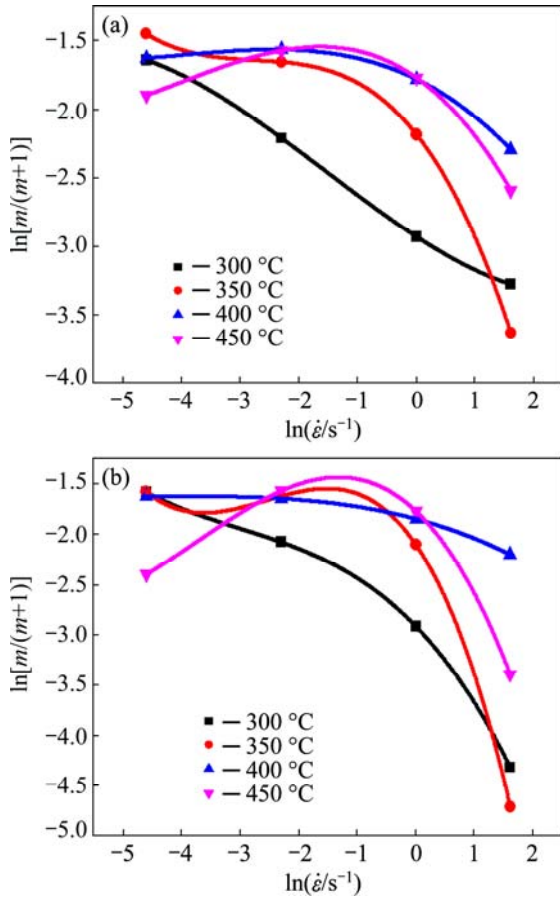


Fig. 4 Relationship between  $\ln[m/(m+1)]$  and  $\ln \dot{\epsilon}$  under strains of 0.2 (a) and 0.4 (b)

### 3.3 Processing maps

The 2D processing maps of the Al–9.0Mg–0.5Mn–0.1Ti alloy obtained at the strains of 0.2, 0.4 and 0.6 are shown in Fig. 5. The contour numbers on the processing maps represent the efficiency of power dissipation ( $\eta$ ) and the shade areas represent the flow instability region where the value of  $\xi(\dot{\epsilon})$  is negative. The other areas represent the safe processing domain. As shown in Fig. 5, it can be obviously found that the efficiency of power dissipation ( $\eta$ ) decreases with increasing the strain rate, and the instability domains have small changes with the development of deformation. It can be seen that the peak values of the power dissipation decrease with the increase of strain, which indicates that strain has a significant effect on the processing maps. As can be seen in Fig. 5(a), the safe processing domain for the Al–9.0Mg–0.5Mn–0.1Ti alloy is in the deformation temperature range of 340–450 °C and the strain rate range of 0.01–0.1 s<sup>-1</sup> at strain of 0.2 with the power

efficiency range of 38%–43%. Similarly, as shown in Fig. 5(c), the safe processing domain is in the deformation temperature range of 320–450 °C and the strain rate range of 0.01–0.1 s<sup>-1</sup> at strain of 0.6 with the power efficiency range of 34%–38%. REDDY et al [20] concluded that the larger the efficiency of power dissipation in this domain, the better the processing of the material at certain deformation condition.

In order to investigate the variation of the efficiency of power dissipation and the deformation conditions, 3D power dissipation maps of Al–9.0Mg–0.5Mn–0.1Ti alloy are shown in Fig. 6. The color of the grid in the 3D

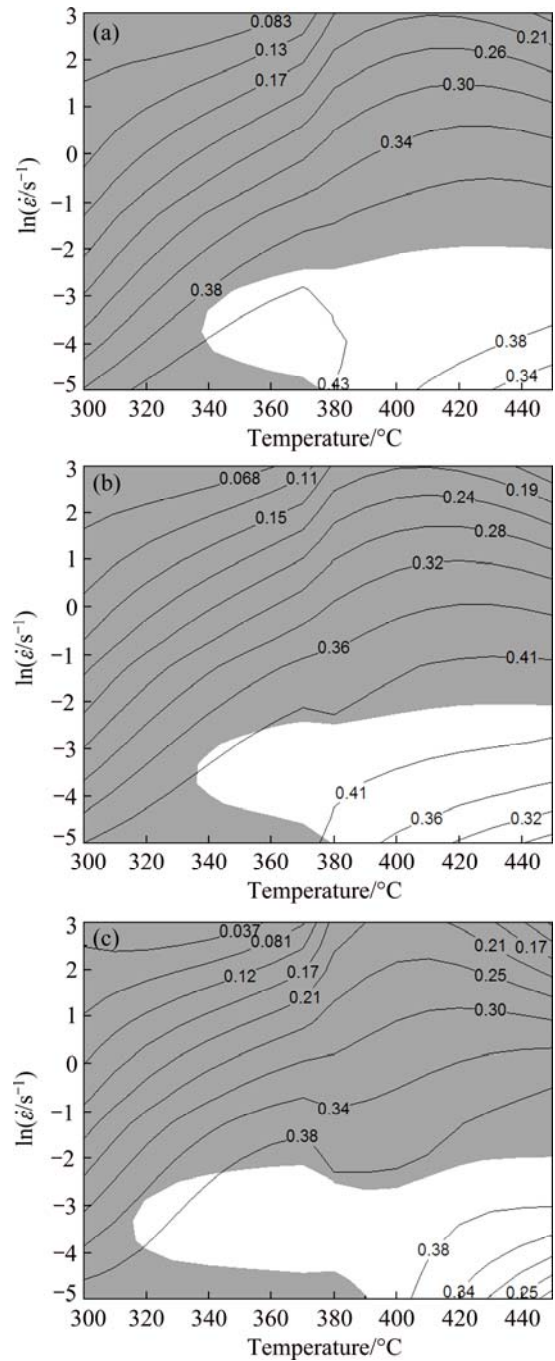
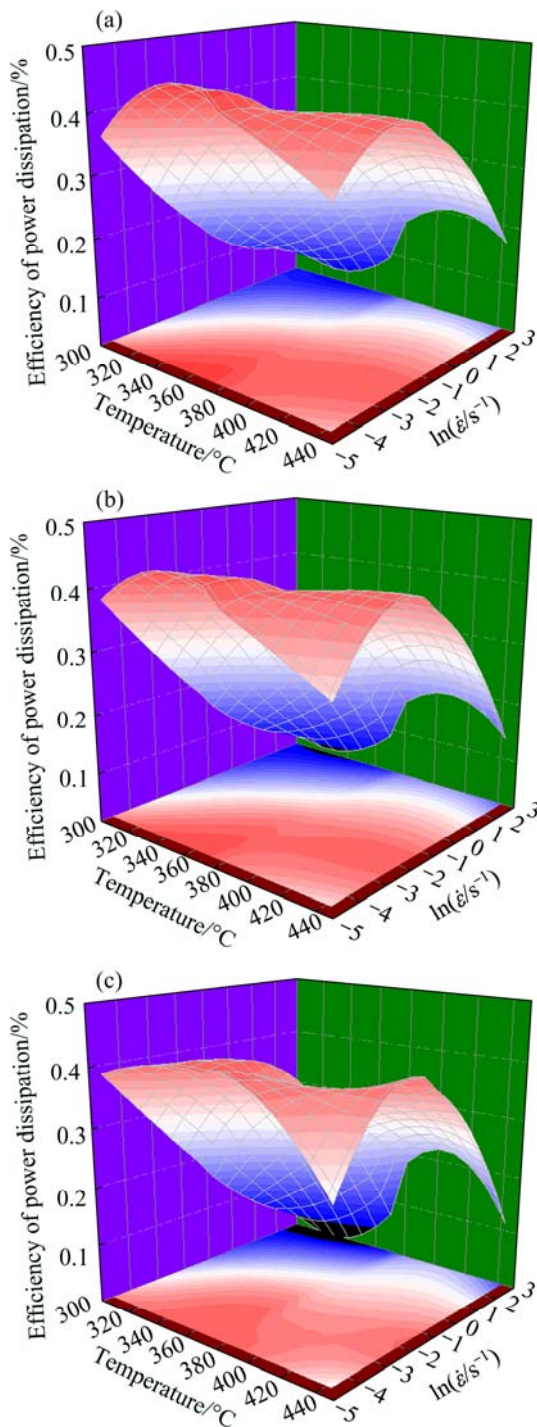


Fig. 5 Hot processing maps of Al–9.0Mg–0.5Mn–0.1Ti alloy under strains of 0.2 (a), 0.4 (b) and 0.6 (c)



**Fig. 6** 3D power dissipation maps of Al-9.0Mg-0.5Mn-0.1Ti alloy from hot compression test at strains of 0.2 (a), 0.4 (b) and 0.6 (c)

power dissipation maps represents the efficiency of power dissipation ( $\eta$ ). As shown in Fig. 6, the deformation temperature, strain rate and strain have significant influence on the efficiency of power dissipation ( $\eta$ ), and the peak values of power dissipation are 0.43, 0.41 and 0.38, respectively. It is observed that the efficiency of power dissipation ( $\eta$ ) decreases with the

increase of strain rate and with the decrease of deformation temperature at strains of 0.2, 0.4 and 0.6. SUN et al [17] investigated the hot deformation behavior of TiAl-based alloy using 3D processing map, where the variation characteristics of the efficiency of power dissipation was in accordance with that in the present work.

In order to investigate the deformation mechanism, the microstructures of Al-9.0Mg-0.5Mn-0.1Ti alloy deformed at different temperatures and strain rates were analyzed. Figure 7 presents the grain morphology, grain boundary and orientation map of the alloy under the compression deformation conditions of strain of 0.4, deformation temperature of 300 °C and strain rate of 1 s<sup>-1</sup>. As shown in Fig. 7(a), the crystal particles are in

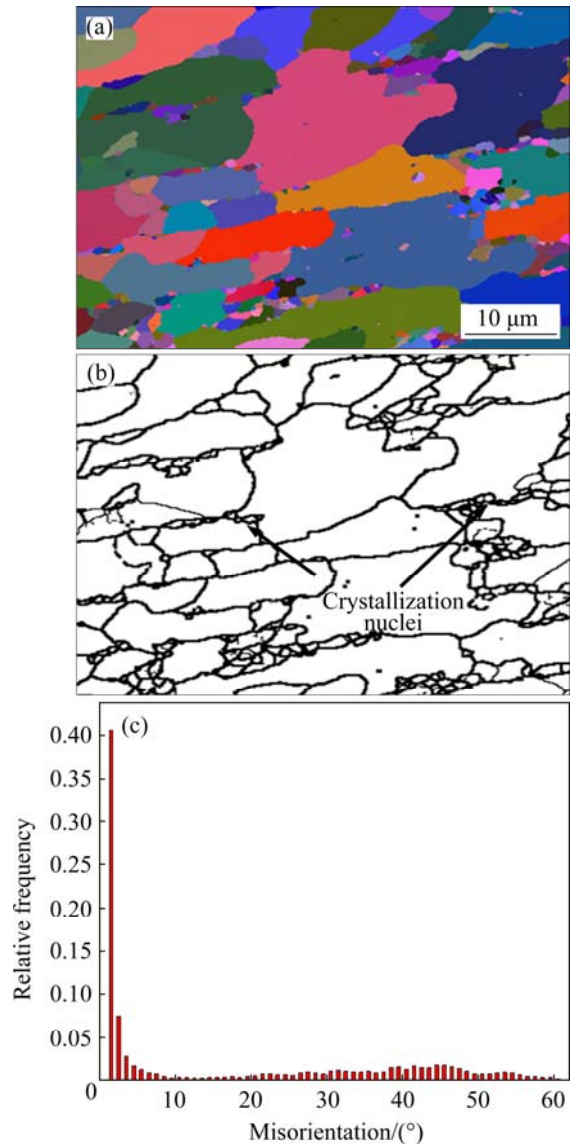


**Fig. 7** EBSD orientation maps of Al-9.0Mg-0.5Mn-0.1Ti alloy deformed at temperature of 300 °C, strain rate of 1 s<sup>-1</sup> and strain of 0.4: (a) Grain morphology map; (b) Grain boundary map; (c) Grain orientation distribution diagram

flat shape and the orientation is mainly in a same direction when the alloy is deformed at low temperature and high strain rate. Furthermore, as shown in Figs. 7(b) and (c), a small amount of recrystallization cores appear at the partially elongated grain boundary, and the portion of high-angle ( $>15^\circ$ ) grain boundaries only accounts for 34%. Figure 8 presents the corresponding results for the alloy under the compression deformation conditions of strain of 0.4, deformation temperature of  $400^\circ\text{C}$  and strain rate of  $0.1\text{ s}^{-1}$ . As can be seen in Fig. 8(a), the crystal particles present equiaxed shape when the test alloy is deformed at high temperature and low strain rate. Compared with Fig. 7, the grains are significantly finer, the structure of the crystal is more uniform and the portion of high-angle grain boundary increases to 86.5%. It is indicated that complete recrystallization has

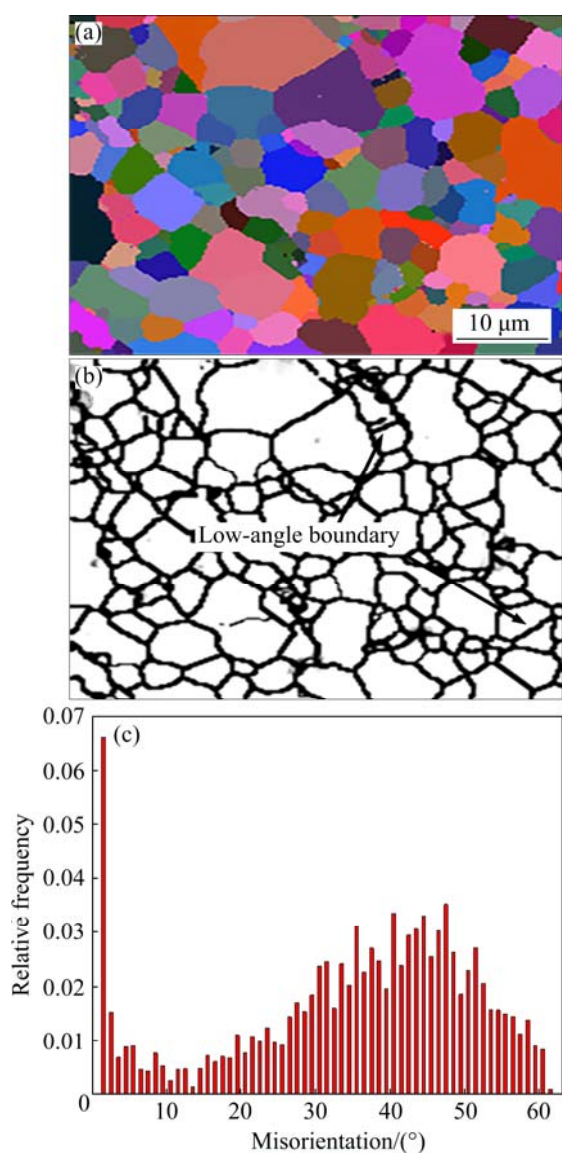


**Fig. 8** EBSD orientation maps of Al-9.0Mg-0.5Mn-0.1Ti alloy deformed at temperature of  $400^\circ\text{C}$ , strain rate of  $0.1\text{ s}^{-1}$  and strain of 0.4: (a) Grain morphology map; (b) Grain boundary map; (c) Grain orientation distribution diagram

occurred in the alloy, and a small amount of low-angle grain boundaries are formed mainly due to the division of grain particles by dislocation wall in the grains, as shown with the arrow in Fig. 8(b).

During the deformation process at low temperatures and high strain rates, the softening mechanism of the test alloy is mainly dynamic recovery due to the low deformation temperature. And the deformation time is so short that the cross slipping and climbing of the dislocation are difficult to occur. Therefore, the dynamic recovery is limited and it is impossible to form grain sub-boundaries, which leads to an extreme increase of the density of dislocation. As a result, the main mechanism at low temperatures and high strain rates is work hardening. When the test alloy is deformed at high temperatures and low strain rates, the softening mechanism of the alloy is a combination of dynamic recovery and dynamic recrystallization. Due to the long deformation time, the cross slipping and the dislocation climbing can completely happen and the recrystallization cores can fully grow up on the basis of a great number of grain sub-boundaries. Thus, the alloy undergoes fully dynamic recrystallization and the softening mechanism can mainly be concluded as dynamic recrystallization. LI et al [21] investigated the hot deformation behavior and microstructure evolution of Al-Cu-Li alloy, and found that the power dissipation of microstructure evolution increases with the increase of  $\eta$ , and the maximum value of  $\eta$  appears in the region of dynamic recrystallization. Similar results are obtained in the present work. The maximum value of  $\eta$  achieves at the deformation temperature of  $400^\circ\text{C}$  and the strain rate of  $0.1\text{ s}^{-1}$ , while the minimum value lies at  $300^\circ\text{C}$  and  $1\text{ s}^{-1}$ , respectively, as shown in Fig. 6(c). It can be explained that when the test alloy deforms at low temperature and high strain rate, the alloy does not have enough energy for the dynamic recrystallization, which can be satisfied at high deformation temperatures and low strain rates.

According to the above analysis, the deformation temperature and strain rate show a remarkable effect on the dynamic recrystallization, which takes place at high deformation temperatures and low strain rates. The dynamic recrystallization can effectively optimize the microstructure of spray-formed Al-9.0Mg-0.5Mn-0.1Ti alloy. Moreover, according to the processing maps and microstructure evolution, it can be successfully deduced that the optimum processing conditions are located in the deformation temperature range of  $340\text{--}450^\circ\text{C}$  and the strain rate range of  $0.01\text{--}0.1\text{ s}^{-1}$  with the power efficiency range of 38%–43%.

## 4 Conclusions

- 1) Hot deformation behavior of the extrusion

preform of spray-formed Al–9.0Mg–0.5Mn–0.1Ti alloy and its microstructure evolution during the isothermal compression deformation were investigated in the deformation temperature range of 300–450 °C and the strain rate range of 0.01–10 s<sup>-1</sup>. The results showed that the flow stress behaviors of Al–9.0Mg–0.5Mn–0.1Ti alloy were greatly influenced by deformation temperature, strain rate and strain.

2) Based on the experimental data, 2D processing maps and 3D power dissipation maps were developed for the extrusion preform of spray-formed Al–9.0Mg–0.5Mn–0.1Ti alloy. The efficiency of power dissipation ( $\eta$ ) decreased with the increase of strain rate and with the decrease of deformation temperature at strains of 0.2, 0.4 and 0.6.

3) Microstructure observations illustrated that dynamic recrystallization takes place at high deformation temperatures and low strain rates during the hot deformation process. The hot processing map indicated that the optimum processing conditions for the extrusion preform of spray-formed Al–9.0Mg–0.5Mn–0.1Ti alloy are in the deformation temperature range of 340–450 °C and the strain rate range of 0.01–0.1 s<sup>-1</sup> with the power efficiency range of 38%–43%.

## References

- [1] FENG Yan, LI Xiao-gen, WANG Ri-cu, PENG Chao-qun, LIU Li. Influence of cerium on microstructures and electrochemical properties of Al–Mg–Sn–Hg anode materials for seawater battery [J]. *Journal of Rare Earths*, 2015, 33(9): 1010–1016.
- [2] WILLIAMS J C, STARKE E A. Progress in structural materials for aerospace systems [J]. *Acta Materialia*, 2003, 51: 5775–5799.
- [3] TOLGA D, COSTAS S. Recent developments in advanced aircraft aluminium alloys [J]. *Materials and Design*, 2014, 56: 862–871.
- [4] DU Gang, YANG Wen, YAN De-sheng, RONG Li-jian. Hardening behavior of the as-cast Al–Mg–Sc–Zr alloy [J]. *Acta Metallurgica Sinica*, 2011, 47(3): 311–316. (in Chinese)
- [5] DAI S L, DELPLANQUE J P, LAVERNIA E J. Microstructural characteristics of 5083 Al alloys processed by reactive spray deposition for net-shape manufacturing [J]. *Metallurgical and Materials Transactions A*, 1998, 29(10): 2597–2611.
- [6] CHEN Zheng-hua, FAN Cai-he, CHEN Zi-gang, CHEN Deng. Densification of large-size spray-deposited Al–Mg alloy square preforms via a novel wedge pressing technology [J]. *Materials Science and Engineering A*, 2009, 506(1–2): 152–156.
- [7] CHEN Zheng-hua, ZHAN Mei-yan, XIA Wei-jun. Putting on the squeeze to improve porous metal density [J]. *Metal Powder Report*, 2004, 59(9): 40–42, 45–47.
- [8] HOGG S C, PALMER I G, THOMAS L G. Processing, microstructure and property aspects of a spraycast Al–Mg–Li–Zr alloy [J]. *Acta Materialia*, 2007, 55(6): 1885–1894.
- [9] ZHA M, LI Y J, MATHIESEN R H, ROVEN H J. Microstructure evolution and mechanical behavior of a binary Al–7Mg alloy processed by equal-channel angular pressing [J]. *Acta Materialia*, 2015, 84: 42–54.
- [10] JOBBA M, MISHRA R K, NIEWCZAS M. Flow stress and work-hardening behaviour of Al–Mg binary alloys [J]. *International Journal of Plasticity*, 2015, 65: 43–60.
- [11] SHEIKH H, SERAJZADEH S. Estimation of flow stress behavior of AA5083 using artificial neural networks with regard to dynamic strain ageing effect [J]. *Journal of Materials Processing Technology*, 2008, 196: 115–119.
- [12] WANG Zhan-feng, ZHANG Hao, CHEN Zheng-hua. Flow stress behaviors of spray deposited 5A06 aluminum alloy under hot compression deformation [J]. *Transactions of Nonferrous Metals Society of China*, 2006, 16(11): 1938–1944.
- [13] LUO J, LI M Q, MA D W. The deformation behavior and processing maps in the isothermal compression of 7A09 aluminum alloy [J]. *Materials Science and Engineering A*, 2012, 532(3): 548–557.
- [14] LI Hui-zhong, WEI Xiao-yan, OUYANG Jie, JIANG Jun, LI Yi. Hot deformation behavior of extruded AZ80 magnesium alloy [J]. *Transactions of Nonferrous Metals Society of China*, 2013, 23: 3180–3185.
- [15] QUAN G Z, WANG Y, YU C T. Hot workability characteristics of as-cast titanium alloy Ti–6Al–2Zr–1Mo–1V: A study using processing map [J]. *Materials Science and Engineering A*, 2013, 564(13): 46–56.
- [16] LIU Juan, CUI Zhen-shan, LI Cong-xin. Analysis of metal workability by integration of FEM and 3D processing maps [J]. *Journal of Materials Processing Technology*, 2008, 205(1): 497–505.
- [17] SUN Y, HU L X, REN J S. Investigation on the hot deformation behavior of powder metallurgy TiAl-based alloy using 3D processing map [J]. *Materials Characterization*, 2015, 100(4): 163–169.
- [18] CAO X W, XU G F, DUAN Y L, YIN Z M, LU L Y, WANG Y J. Achieving high superplasticity of a new Al–Mg–Sc–Zr alloy sheet prepared by a simple thermal-mechanical process [J]. *Materials Science and Engineering A*, 2015, 647: 333–343.
- [19] WANG Chun-xia, XU Fu-xiao, ZHAO Da-zhi, ZHAO Xiang, ZUO Liang. Hot deformation and processing maps of DC cast Al–15%Si alloy [J]. *Materials Science and Engineering A*, 2013, 577(11): 73–80.
- [20] LIU W, ZHAO H, LI D. Hot deformation behavior of AA7085 aluminum alloy during isothermal compression at elevated temperature [J]. *Materials Science and Engineering A*, 2014, 596(4): 176–182.
- [21] LI Bo, PAN Qing-lin, YIN Zi-min. Characterization of hot deformation behavior of as-homogenized Al–Cu–Li–Sc–Zr alloy using processing maps [J]. *Materials Science and Engineering A*, 2014, 614(4): 199–206.

## 基于加工图的 Al-9.0Mg-0.5Mn-0.1Ti 合金的热变形行为

范才河<sup>1,2</sup>, 彭英彪<sup>1</sup>, 阳海棠<sup>1</sup>, 周伟<sup>1</sup>, 严红革<sup>2,3</sup>

1. 湖南工业大学 冶金与材料工程学院, 株洲 412007;
2. 湖南大学 喷射沉积技术及应用湖南省重点实验室, 长沙 410082;
3. 湖南大学 材料科学与工程学院, 长沙 410082

**摘 要:** 采用等温热压缩试验研究不同变形条件下(变形温度 300~450 °C、应变速率 0.01~10 s<sup>-1</sup>)喷射成形 Al-9.0Mg-0.5Mn-0.1Ti 合金挤压坯的流变应力行为, 并基于动态材料模型建立 2D 加工图和 3D 功率耗散图来分析合金的流变失稳区和优化合金的热变形工艺参数。结果表明, 当应变为 0.4 时, 合金在 300 °C、1 s<sup>-1</sup> 条件下压缩变形, 能量耗散效率因子  $\eta$  值最小, 主要软化机制为动态回复, 晶粒呈扁平状, 大角度晶界(>15°)约占 34%; 合金在 400 °C、0.1 s<sup>-1</sup> 条件下压缩变形, 能量耗散效率因子  $\eta$  值最大, 合金的主要软化机制为动态再结晶, 组织为完全再结晶组织, 大角度晶界(>15°)约占 86.5%。2D 加工图和 3D 功率耗散图表明喷射成形 Al-9.0Mg-0.5Mn-0.1Ti 合金挤压坯的最佳变形条件是: 变形温度 340~450 °C、应变速率 0.01~0.1 s<sup>-1</sup>, 合金的能量耗散系数 38%~43%。

**关键词:** 喷射成形; Al-9.0Mg-0.5Mn-0.1Ti 合金; 热压缩变形; 加工图; 动态再结晶

(Edited by Sai-qian YUAN)